Compressible solvers for combustion noise simulations

By A. L. Birbaud AND H. Pitsch

1. Motivation and objectives

The ultimate objective of the present study is to assess the role of direct and indirect noise generated by the unsteady heat release in aircraft engines, and to determine its influence on the sound radiated from the combustion chamber. Previous studies indicated that noise computations require numerical schemes of high-order accuracy to resolve the high-frequency components of the noise spectrum. As a first step in the study noise radiation in complex confined systems, we have focused on canonical flows, where the influence of the configuration and physical parameters can be systematically investigated.

The code used in this study is the NGA flow solver developed at Stanford University, which is based on a variable density, low Mach formulation (Desjardins *et al.*, 2007). This flow solver has the capability to perform large-eddy simulations (LES) of reactive and multi-phase flows. Other advantages of the structured code are that it is very efficient and that the discretization allows for higher order accurate formulations of the spatial derivatives.

In order to investigate the fundamental aspects of combustion noise, fully compressible LES are envisaged. A compressible capability has been added to the NGA code to compute the noise in the combustion chamber. Several methods are available to solve the compressible Navier-Stokes equations, with different time-integration methods and spatial discretizations. Two methods are tested in the present study. Their general properties are discussed first, and the capability of the solver retained to simulate combustion noise is then considered.

2. Numerical methods

The two solvers compared in this study are the fractional-step method developed by Moureau *et al.* (2007), and a modified form of an iterative solver by Hou & Mahesh (2005).

2.1. *The fractional-step method*

The fractional-step method by Moureau *et al.* (2007) is based on a characteristic splitting of the Navier-Stokes equations into two steps. The first step is the advection of the conservative variables ϕ at the convective velocity:

$$\frac{\phi_i^* - \phi_i^t}{\Delta t} + \frac{\partial}{\partial x_j}(\phi_i^{t+\frac{1}{2}} u_j^{t+\frac{1}{2}}) - \phi_i^{t+\frac{1}{2}} \frac{\partial}{\partial x_j} u_j^{t+\frac{1}{2}} = D_\phi \,. \tag{2.1}$$

In the second step, the variables are corrected by the pressure residual coming from the solution of the Helmholtz equation:

$$\frac{\partial^2}{\partial x_j^2}\delta p_j - \frac{\partial}{\partial x_j}\left(\frac{2\delta p_j u_j^{t+\frac{1}{2}}}{c_j^2 \Delta t}\right) - \frac{4\delta p_i}{c_i^2 \Delta t} = -\frac{\partial^2}{\partial x_j^2}(p_i^* + p_i^t)$$

$$+\frac{4}{\Delta t}\left(\frac{\rho_i^* - \rho_i^t}{\Delta t} + \frac{\partial}{\partial x_j}\frac{g_j^* + g_j^t}{2}\right).$$

The Helmholtz equation is obtained by taking the divergence of the momentum-correction equation:

$$\frac{g_i^{t+1} - g_i^t}{\Delta t} - \frac{u_i}{c_i^2}\frac{\delta p_i}{\Delta t} = -\frac{\partial}{\partial x_i}\left(\frac{p_i^{t+1} + p_i^t}{2}\right), \tag{2.2}$$

and the unknown quantity g_i^{t+1} is removed by using the continuity equation, ensuring mass conservation. A second-order temporal discretization scheme is used with two inner-loop iterations. In this case, all variables are collocated in time. The spatial discretization is performed using the operators described by Morinishi *et al.* (1998), and is also of second-order accuracy. This method has the advantage of being very efficient, as shown by Moureau *et al.* (2007), and has been used to calculate low-frequency combustion stability on unstructured meshes.

2.2. *The predictor-corrector method*

The predictor-corrector method proposed by Hou & Mahesh (2005) was originally developed as a collocated finite-volume formulation to allow for an easy extension to unstructured grids. In this approach, the discrete divergence is constrained by the energy equation ensuring that the total energy is discretely conserved. The method is non-dissipative and fully implicit, which makes it well-suited for applications with time steps on the order of the convective time scale.

The non-reactive Navier-Stokes equations, density, momentum and energy are first expressed in terms of a predicted quantity, which is later corrected by the pressure residual obtained after the solution of the system between two subiterations. The outer loop is initialized using the quantities calculated at the previous time step.

The density equation is advanced first using the best approximation for the velocity field:

$$\frac{\rho^{t+\frac{3}{2}} - \rho^{t+\frac{1}{2}}}{\Delta t} + \frac{\partial \rho^{t+1} u_j^{t+1}}{\partial x_j} = 0. \tag{2.3}$$

The momentum equation is then advanced using:

$$\frac{g_i^* - g_i^t}{\Delta t} + \frac{\partial g_i^{t+\frac{1}{2}} u_j^{t+\frac{1}{2},k}}{\partial x_j} = -\frac{1}{4}\frac{\partial}{\partial x_i}\left[p^{t-\frac{1}{2}} + 2p^{t+\frac{1}{2}} + p^{t+\frac{3}{2},k}\right] + \frac{\partial \tau_{ij}^{t+\frac{1}{2},k}}{\partial x_j}, \tag{2.4}$$

where $g_i = \rho u_i$, starred quantities correspond to predicted quantities, and k refers to the number of subiterations. Due to the staggering in time, all scalar variables are advanced between $t + \frac{1}{2}$ and $t + \frac{3}{2}$, and the velocity between t and $t + 1$. The predictor step is the difference between the previous equations and the exact equations, and yields a formulation for the correction of velocity and momentum based on the pressure residual

$$p^{t+\frac{3}{2},k+1} = p^{t+\frac{3}{2},k} + \delta p, \tag{2.5}$$

$$g_i^{t+1,k+1} = g_i^* - \frac{\Delta t}{4}\frac{\partial \delta p}{\partial x_i}, \tag{2.6}$$

$$u_i^{t+1,k+1} = u_i^* - \frac{\Delta t}{4\rho^{t+1}}\frac{\partial \delta p}{\partial x_i}. \tag{2.7}$$

These expressions are then introduced into the discrete energy equation and linearized

in δp, which, assuming constant γ, yields:

$$\begin{aligned}\frac{\delta p}{2\Delta t} - \frac{\gamma-1}{4}\rho^{t+1}\frac{\partial \delta p}{\partial x_i}\frac{u_i^*}{\rho^{t+1}} + \frac{\partial}{\partial x_j}[\frac{\gamma}{4}\delta p u_j^{t+\frac{1}{2},*} - \frac{\gamma}{2}\bar{p}^t\frac{\Delta t}{4\rho^{t+1}}\frac{\partial \delta p}{\partial x_j} \\ -\frac{\gamma-1}{2}\rho^{t+\frac{1}{2}}u_i^{t+\frac{1}{2},*}u_i^{t+\frac{1}{2},*}\frac{\Delta t}{8\rho^{t+1}}\frac{\partial \delta p}{\partial x_j} \\ -\frac{\gamma-1}{2}\rho^{t+\frac{1}{2}}\frac{\Delta t}{4\rho^{t+1}}\frac{\partial \delta p}{\partial x_i}u_i^{t+\frac{1}{2},*}u_j^{t+\frac{1}{2},*}] \\ = -\frac{1}{2\Delta t}(p^{t+\frac{3}{2},k} - p^{t-\frac{1}{2}}) - \frac{\gamma-1}{2\Delta t}\left[\rho^{t+1}u_i^*u_i^* - \rho^t u_i^t u_i^t\right] \\ -\frac{\partial}{\partial x_j}[\gamma\bar{p}^t u_j^{t+\frac{1}{2},*} + \frac{\gamma-1}{2}\rho^{t+1}u_i^{t+\frac{1}{2},*}u_i^{t+\frac{1}{2},*}u_j^{t+\frac{1}{2},*}] \\ +(\gamma-1)\frac{\partial u_i \tau_{ij}^{t+\frac{1}{2},k}}{\partial x_j} + \frac{Cp}{Pr}\frac{\partial^2 T^{t+\frac{1}{2}}}{\partial x_j \partial x_j}\,.\end{aligned}$$

The resulting energy equation is solved using a bi-conjugate gradient method. The convergence on all the residuals is checked before moving to the next time step. The formulation is fully implicit and therefore is not restricted by the acoustic CFL number. The solver is also able to handle high Mach number flows.

2.3. *Comparison of the two methods*

The two methods are compared here on the basis of 1-D test cases. For the fractional-step method, both collocated (FSC) and staggered (FSS) arrangement of the variables in space are considered. All quantities are collocated in time. For the predictor-corrector method (PC), the variables are staggered in space and time. The temporal and spatial discretizations are of second-order accuracy. The stability, computational cost and accuracy of the solvers are investigated below.

2.3.1. *Perturbation signals*

For all test cases discussed in this study, the mean flow velocity is set to unity and the velocity, pressure and density perturbations are set according to

$$u(x) = \sin\left(\frac{2\pi x}{a\Delta x}\right)\exp\left[-\ln 2\left(\frac{x}{b\Delta x}\right)^2\right], \tag{2.8}$$

$$p(x) = P_0 + \rho_0 c_0 u(x)\,, \tag{2.9}$$

where a and b are parameters determining the resolution of the signal in Fourier space. This perturbed signal shape corresponds to problem (I) used by Bogey & Bailly (2004) to study acoustic propagation over large distances. The parameters a and b can be adjusted to modify the resolution of the dominant wavelength and the half-width of the Gaussian function, respectively. Test cases based on this perturbation signal include the long-range propagation of 1-D disturbances allowing for the characterization of the dispersion and dissipation errors.

2.3.2. *Results*

The computational domain is discretized initially using 64 grid points with periodic boundary conditions. The CFL number, based on the speed of sound, is first set to 0.1. Figure 1 shows the evolution of the kinetic energy integrated over the domain as a function of time. For the space-staggered formulations, the velocity is interpolated to cell centers

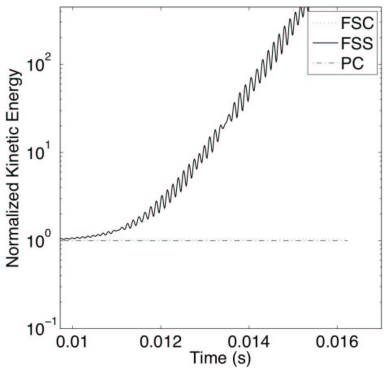

FIGURE 1. Evolution of the normalized integrated kinetic energy as a function of time. Comparison between the fractional-step method proposed by Moureau *et al.* (2007) on collocated and staggered grids, and the staggered predictor-corrector scheme of Hou & Mahesh (2005).

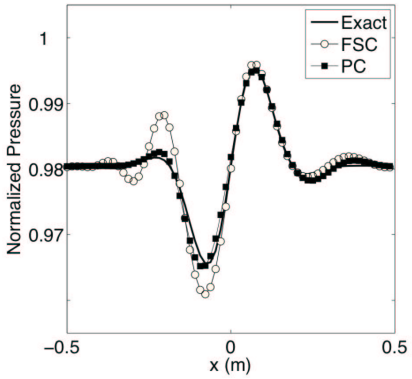

FIGURE 2. Pressure signals obtained after one flow passing time. Comparison of the FSC and PC methods to the exact solution.

before evaluating the kinetic energy. Results indicate that with the chosen operators, the space-staggered formulation of the fractional step scheme (FSS) is unstable, whereas the space-collocated (FSC) scheme conserves kinetic energy. The plot in Fig. 1 also shows that the predictor-corrector method conserves kinetic energy. This first test indicates that the FSS method is not compatible with the present space-staggered formulation it will not be discussed any further in the present study. The next test case compares pressure signals obtained with the FSC and PC methods after the signal has been advected by one period. Figure 2 shows that the pressure signals obtained with the PC method are better than results obtained with the FSC method due to the difference between staggered and collocated discretizations (where on the same mesh, the staggered formulation increases the accuracy [Bogey & Bailly (2004); Colonius & Lele (2004)]).

Next, we compare the computational cost of the two approaches. One of the advantages of the FSC method is that only two inner-loop iterations are necessary to achieve second-order temporal accuracy. As the FSC solver is semi-implicit because of the implicit solution of the Helmholtz equation that advances the pressure fluctuations, the time step is not constrained by the acoustic CFL limit. This is also the case for the

Method	Continuity	Momentum	Pressure iterations	Subiterations (outer loop)
FSC CFL = 0.1	2	2	2	2
FSC CFL = 0.7	2	2	4	2
PC CFL = 0.1	2	2	3	4
PC CFL = 0.7	2	2	6	4

TABLE 1. Computational cost in number of iterations of the FSC and PC methods. Tests are carried out on problem C2 with $a = 41$ and $b = 13$. The convergence criterion is set to 10^{-15}, and the convergence on the pressure residual for the FC method is set to 10^{-10}.

PC method, which is fully implicit. However, the number of subiterations necessary to converge all the residuals is higher for the PC solver than for the FSC method. This is shown in Table 1, where the computational cost of the two solvers for two different CFL numbers is compared.

The results indicate that for a simple 1-D test case, the PC method is at least twice as expensive as the FSC method. This factor increases as the simulation becomes more complex. For example, 10 subiterations are required for the PC method to converge all quantities for a channel flow. In the case of even more complex flows, the number of subiterations required remains less than 15 for the configurations tested, which include compressible Homogeneous Isotropic Turbulence (not discussed in this study). The number of subiterations required by the PC method to converge, although relatively high compared to the FSC method, remains lower than other iterative approaches, for example, the scheme by Wall, Pierce & Moin (2002).

From these comparisons, FSC is found to be less expensive but also less accurate than the PC method. It is well-suited to compute complex flows where the frequencies of interest remain in the low range. In this limit, the number of grid points per acoustic wavelength is such that the waves are correctly transported in the computational domain, and unresolved frequencies are dissipated. Therefore, the approach is particularly applicable to simulating low-frequency phenomena, such as combustion instabilities. For noise applications, it is crucial to propagate smaller acoustic wavelengths, or higher frequencies accurately in the domain. Even though less efficient, the PC method, which is staggered in space and time, is therefore more appropriate. The ability of the PC solver to transport acoustic waves is examined next.

3. Combustor-type test case

From the previous test cases, the PC method has been chosen for the combustion noise simulations. It is interesting to perform tests that mimic the wave characteristics are close to those found in a combustion chamber.

Here we will again use the perturbed pressure and velocity signals proposed by Bogey & Bailly (2004) previously described to propagate acoustic waves in a fictitious 1-D combustor. Based on experiments conducted by Bake *et al.* (2007), in the configuration schematically shown in Fig. 3, power-spectral densities of the pressure signals in the combustion chamber indicate that the dominant modes are usually smaller than 5000 Hz. Given the speeds of sound in the fresh stream and in the hot combustion products, this corresponds to certain wavelengths of the perturbations provided by $\lambda = c/f$. With a limit frequency of the order of 10^4 Hz, the shortest wavelength in the non-reactive case, where $c \simeq 346\,\mathrm{m/s}$ for $T_0 = 298\,\mathrm{K}$ and $\rho = 1.18\,\mathrm{kg/m^3}$, is then $\lambda_c = 0.0347\,\mathrm{m}$.

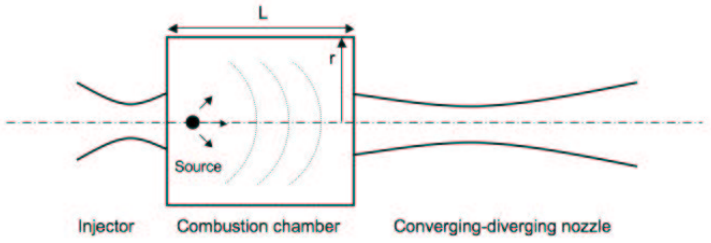

FIGURE 3. Schematic description of test geometry.

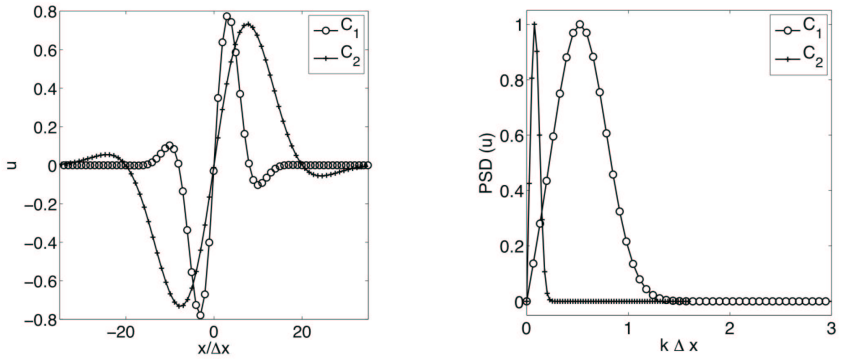

FIGURE 4. Left: Initial velocity perturbation signals. Right: Initial velocity perturbation power spectral density. C_1 refers to the case $T_0 = 298\,\mathrm{K}$, $a = 16$, $b = 6$, and C_2 refers to $T_0 = 2000\,\mathrm{K}$, $a \simeq 41$ and $b = 13$.

In a reactive situation with $c \simeq 897.5\,\mathrm{m/s}$ for $T_0 = 2000\,\mathrm{K}$ and $\rho = 0.17\,\mathrm{kg/m^3}$, $\lambda_h = 0.0897\,\mathrm{m}$. If the flame is assumed to be a monopole noise source located close to the inlet plane in the combustion chamber, a characteristic length scale of the problem is the chamber length L corresponding to the larger typical propagation distance for the acoustic waves. As the waves reflect on the wall in the outlet plane, it is possible to define a reference length $2L$ accounting for the propagation of a reflected acoustic wave. The domain length is therefore set to $2L = 0.23\,\mathrm{m}$ based on the configuration by Bake *et al.* (2007) with periodic boundary conditions in the axial direction. The flow is initialized with the perturbation proposed by Bogey & Bailly (2004) in the center of the domain. The frequency f is set to 10,000 Hz, and the parameters a and b are chosen to have 16 points per dominant wavelength in the non-reactive case. As $a\Delta x = c/f$, this gives a value for Δx of $2.2 \cdot 10^{-3}\,\mathrm{m}$, or 106 grid points in the domain. Keeping Δx constant, as the temperature is increased to $T_0 = 2000\,\mathrm{K}$ gives $a \simeq 41$ for the hot case. The parameter b is set to 6 and 13 for the cold and hot cases, respectively. The initial shapes and spectra of the two perturbations are shown in Fig. 4. Note that the limit frequency chosen here is particularly restrictive, even though the speed of sound is uniform over the domain and the grid spacing is regular. To evaluate the quality of the results, pressure and velocity signals are shown after a given number of flow-through times corresponding to a number of wave reflections. Figures 5 and 6 show the results obtained for the cold (C_1) and hot flow (C_2) simulations, respectively, for a second-order spatial discretization. Data shown in Fig. 5 correspond to pressure signals obtained after 1 to 8 reflections for two different

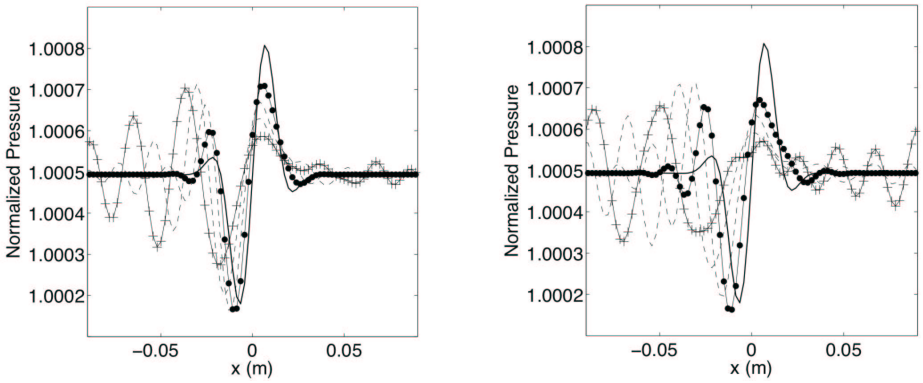

FIGURE 5. Pressure signals after a given number of flow-through times, for the cold case (C_1). Solid line: exact solution, • calculated solution after 1 reflection, + calculated solution after 8 reflections. Dashed lines: calculated solutions after 2 and 4 reflections. Left: CFL = 0.1. Right: CFL = 0.7.

CFL numbers. In the case of a small acoustic CFL number, the original perturbed signal is already deformed after one reflection. The maximum amplitude has decreased and a small phase-shift is observed. The signal shape, however, is globally conserved. As the number of reflections is increased, strong oscillations are observed corresponding to the dispersion introduced by the solver. The signal shape is no longer preserved, and as the solver is non-dissipative, the oscillations remain in the domain even after long computational times. As this CFL value minimizes the temporal error, increasing the time step to a more reasonable value leads to the curves shown in Fig. 5 (right). In this case, even after one reflection the pressure signal is very different from the exact signal. Strong oscillations are observed for more than one reflection. With 16 points per dominant wavelength, the second-order scheme is not able to propagate the acoustic waves accurately, even for one reflection. Note that one reflection corresponds to the propagation of 6 times the dominant wavelength, as this is the quantity usually considered to assess the quality of the solvers (as used by Bogey & Bailly (2004)). Given that, considering two reflections is equivalent to examining the propagation after 12 perturbation wavelengths. It is usually found that higher-order low dispersive schemes are necessary to obtain acceptable results after 10 propagation wavelengths, as mentioned by Bogey & Bailly (2004). However, it is interesting to consider this issue from a more physical perspective as it is directly connected to what can be expected in an actual simulation.

Results displayed in Fig. 6 correspond to the high-temperature type simulation (C_2). As Δx has been kept constant and the temperature increased, the dominant wavelength is now discretized by 41 grid points. As the speed of sound is also much higher than for the previous test case, the time required for the wave to propagate over one reflection has decreased. The combination of these two factors leads to an improvement of the results for the two CFL numbers calculated. For small time steps and small propagation distances, reasonable agreement is obtained between the calculated and the exact solutions. For larger time steps, no large oscillations are observed, but the waves are dispersed after two reflections. The phase-shift observed after 12 reflections due to the error on the wave propagation is not acceptable, if this component contributes to the noise generation in the combustion chamber.

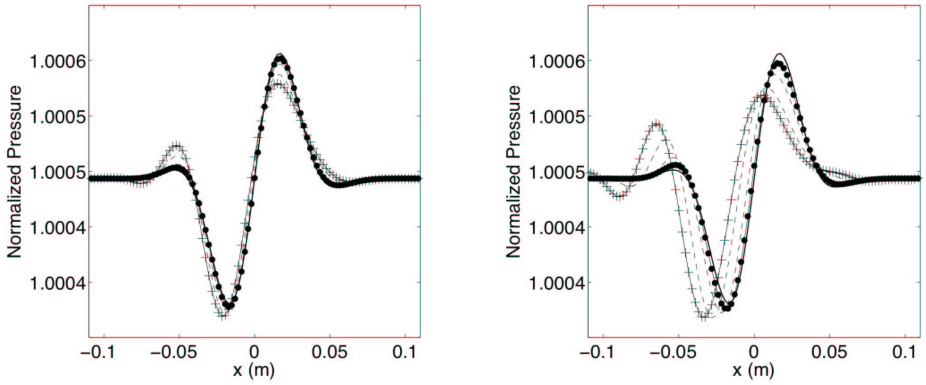

FIGURE 6. Pressure signals over the domain after a given number of flow-through times, $a = 41$ and $b = 13$. Solid line: exact solution, • calculated solution after 2 reflections, + calculated solution after 12 reflections. Dashed lines: calculated solutions after 4 and 8 reflections. Left: CFL = 0.2. Right: CFL = 0.7.

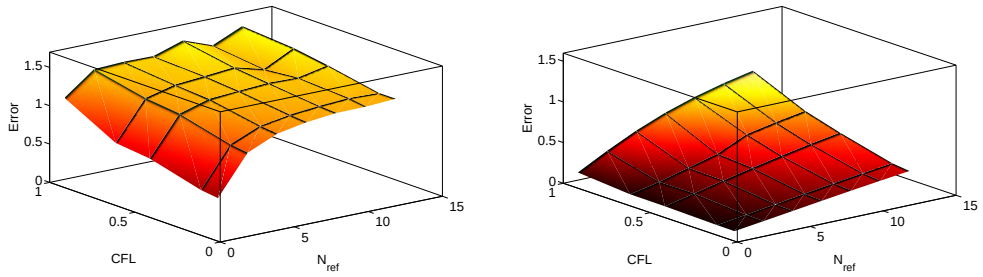

FIGURE 7. Evolution of the error as a function of the acoustic CFL and reflection (N_{ref}) numbers. Left: case C_1. Right: case C_2.

It is now interesting to quantify this error and consider its evolution as a function of both the reflection and CFL numbers. To characterize the signals with respect to the exact solution, the quantity considered is given as:

$$err^2 = \frac{\sum_{n=1}^{n_x}(p_{calc} - p_{ex})^2}{\sum_{n=1}^{n_x}(p_{ex} - \overline{p_{ex}})^2}\,. \tag{3.1}$$

This error can be seen as the RMS of the difference signal between the computed and exact solutions normalized by the RMS value of the exact signal. The quantity *err* tends to zero as the calculations get close to the exact solution and to a finite value in the opposite situation. $err = 1$ indicates that the difference between signals is of the order of the initial perturbation amplitude compared to the mean value. In this case and at this point, results have little meaning. Using this parameter, a systematic study is performed for CFL numbers between 0.1 and 1, and reflection numbers N_{ref} between 1 and 13. The evolution of *err* is shown in Fig. 7 as a function of these quantities for both cold and hot type simulations. As seen by comparing signal shapes, for the cold case, the error is initially high and increases rapidly with CFL and N_{ref}. Even by considering the information that is only relevant, if not accurate, as soon as N_{ref} exceeds 3 and the CFL number is greater than 0.2, *err* becomes larger than unity. This confirms that for 16 grid points per wavelength or lower resolution, the acoustic waves are not correctly

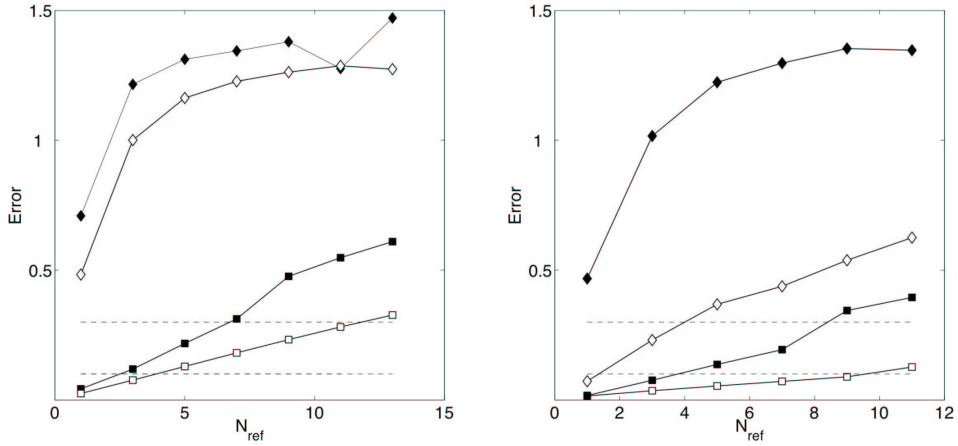

FIGURE 8. Evolution of the error as a function of the reflection (N_{ref}) number. Left: second-order discretization, □ CFL = 0.2 C_2 case, ■ CFL = 0.7 C_2 case, ◊ CFL = 0.2 C_1 case, ♦ CFL = 0.7 C_1 case. Right: fourth-order discretization, □ CFL = 0.2 C_2 case, ■ CFL = 0.7 C_2 case, ◊ CFL = 0.2 C_1 case, ♦ CFL = 0.7 C_1 case. Dashed lines, constant error of 10 and 30%.

transported by the solver. For the C_2 case simulations, the error remains below unity for all N_{ref}, provided that CFL is less than 1. In particular, it is interesting to fix some CFL values, and consider the evolution of *err* as function of N_{ref}. This is done in Fig. 8 (left) for both cases and CFL = 0.1 and CFL = 0.7. Results corresponding to the hot simulation are the square symbols. The dashed lines correspond to *err* = 0.1 and *err* = 0.3. For CFL = 0.2, the error remains below 30% for all the N_{ref}, and below 10% for about 5 reflections. For CFL = 0.7, after 3 reflections, *err* is greater than 0.1, and after 7 reflections it becomes greater than 0.3. This implies that even with 41 grid points per dominant wavelength, a reasonable level of accuracy with the second-order discretization can hardly be achieved for very small time steps.

We compared these curves with similar data obtained with fourth-order spatial discretization, which is shown in Fig. 8 (right). In the cold case with a CFL of 0.2, the error is less than 0.3 for up to 4 reflections, which is dramatically better than the second-order results. For example, for $N_{ref} = 3$, one obtains *err* = 0.92 (second-order) and *err* = 0.24 (fourth-order). If CFL = 0.7, the improvement is not so significant, showing that the waves are still not propagated correctly. In the case of 41 grid points per dominant wavelength, results are largely improved as the error remains below 0.1 for small time steps, and below 0.3 for almost up to 9 reflections and CFL = 0.7.

Previous tests showed that fourth-order accuracy as well as low CFL numbers are required to correctly propagate the acoustic waves with only 16 grid points per dominant wavelength. In a realistic simulation, the speed of sound is expected to vary within the computational domain, and multiple wave reflections will occur during the total simulation time, influencing the flame behavior and the entire pressure field. In the fresh stream, where the speed of sound is much lower than in the hot products, in order to describe approximately five reflections (with the shortest wavelength corresponding to f =10,000 Hz), fourth-order calculations with an acoustic CFL number equal to 0.2 are necessary.

As the temperature is increased, the shortest wavelength corresponding to the same

frequency f=10,000 Hz becomes larger. Thus, with the same grid, the acoustic waves are more resolved, leading to improved results. Given that the frequency used to set the parameters is large compared to the 3000 – 5000 Hz seen in the experiments by Bake *et al.* (2007), the tests conducted with a frequency of 10,000 Hz are particularly challenging for the solver. However, this shows that for aeroacoustic applications in a confined geometry, fully compressible simulations with second-order of spatial accuracy might not provide satisfactory results. Even with a fourth-order discretization, and taking advantage of the space and time staggering of the variables, the use of large time steps leads to inaccurate propagation of the short wavelength acoustic waves, and by that of the high-frequency noise components. This indicates also that fully compressible simulations performed on unstructured grids where schemes are at most third-order accurate can be envisaged but might require a very large number of grid points to overcome this issue.

To combine computational efficiency and reasonable accuracy with the present method, one could compute the flowfield with a higher CFL number, and benefit from the implicit formulation to begin with large time steps. As the simulation reaches the point where the noise characteristics have to be computed, the time step can be decreased to a value for which the propagation is more accurate, and the order of the scheme augmented. Due to the methods low dissipation, the influence of the unresolved waves on the results must be considered. This numerical error might directly influence the computed noise. In addition, with a subgrid-scale model that uses a dynamic procedure, the numerical error due to dispersion contributes to the calculation of the model constants, and by that introduces more error on the simulations. To minimize the numerical noise, one solution (commonly used in aeroacoustics) would be to filter the unresolved frequencies to eliminate their influence on the results, but only on the acoustic field. This could be done by filtering only the potential velocity field to separate hydrodynamics and acoustics before applying the filter.

4. Conclusions and future work

In this study we have examined different methods to simulate compressible flows and the noise radiated in a confined geometry configuration. It was found that the fully implicit method of Hou & Mahesh (2005) implemented with a staggered formulation of the variables and fourth-order order of spatial derivatives on a structured grid was a good compromise between efficiency and accuracy.

This scheme has been added in the NGA flow solver and verified in several 1-D and 2-D test cases. The non-reflective Navier-Stokes Characteristic Boundary Conditions have been included and tested to simulate partially non-reflective outlets and also to introduce, for example, entropy modulation via the domain inlets. Further analysis of entropy wave modulation is currently under investigation. For this, a configuration is used, similar to that proposed by Bake *et al.* (2007) to investigate the effect of modulation amplitude and frequency on the features of the transmitted acoustic wave passing through a converging/diverging nozzle. For the LES computations, the dynamic model used is the one proposed by Moin *et al.* (1991) and the combustion model implemented for reactive calculations (under verification) is the flamelet/progress variable approach by Ihme *et al.* (2005). In order to use this approach to compute complex realistic geometries such as combustion chambers adequate boundary conditions must be included. This issue is currently under investigation, and the immersed boundary method developed by Mittal & Iaccarino (2005); Ghias *et al.* (2007) is being coupled with the compressible solver to

execute complex geometries on a structured mesh. This approach uses the 3-D version of the structured code developed at Stanford University by Desjardins *et al.* (2007), which has been developed and validated for variable density low Mach number flows.

The first step of fundamental interest is to study the interaction between the interface boundaries and acoustic waves. The main issues of the immersed boundary method are the interpolation methods and the local mass conservation across the interface. The available developments for boundary conditions are generally second-order accurate. One remaining task is to test these methods and verify their influence on the global order of the scheme and examine higher-order formulations.

5. Acknowledgments

This work is supported by NASA. The authors gratefully acknowledge the helpful discussions with Drs. A. Giauque and F. Ham.

REFERENCES

Bake, F., Michel, U. & Roehle, I. 2007 Investigation of Entropy Noise in Aero-Engine Combustors. *Transactions of the ASME* **129**, 370–376.

Bogey, C. & Bailly, C. 2004 A family of low dispersive and low dissipative explicit schemes for flow and noise computations. *J. of Comp. Phys.* **194**, 194–214.

Colonius, T. & Lele, S. K. 2004 Computational aeroacoustics: progress on nonlinear problems of sound generation. *Progress in Aerospace Sicences.* **40**, 345–416.

Moin, P., Squires K., Cabot W. and Lee S. 1991 A dynamic subgrid-scale model for compressible turbulence and scalar transport. *Phys. of Fluids. (A).***3**(11), 2746–2757.

Hou, Y. & Mahesh, K. 2005 A robust, collocated, implicit algorithm for direct numerical simulation of compressible, turbulent flows. *J. of Comp. Phys.* **205**, 205–221.

Poinsot, T. & Lele, S. K. 1992 Boundary conditions for direct simulations of compressible viscous flows. *J. of Comp. Phys.* **101**, 104–129.

Wall, C., Pierce, C. D. & Moin, P. 2002 A semi-implicit method for resolution of acoustic waves in low Mach number flows. *J. of Comp. Phys.* **181**, 545–563.

Ihme, M., Cha, C. M. & Pitsch, H. 2005 Prediction of local extinction and re-ignition effects in non-premixed turbulent combustion using a flamelet/progress variable approach. *Proc. of Comb. Inst.* **30**, 793–800.

Moureau, V., Berat, C. & Pitsch, H. 2007 An efficient semi-implicit compressible solver for large-eddy simulations. *J. of Comp. Phys.* **226**(2), 1256–1270.

Desjardins, O., Blanquart, G., Balarac, G. & Pitsch, H. 2007 High-order conservative finite difference scheme for variable density low Mach number turbulent flows. *J. of Comp. Phys.* (submitted).

Mittal, R. & Iaccarino, G. 2005 Immersed Boundary Methods. *Ann. Rev. Fluid. Mech.* **37**, 239–261.

Ghias, R., Mittal, R. & Dong, H. 2007 A sharp interface immersed boundary method for compressible viscous flows. *J. of Comp. Phys.* **225**, 528–553.

Morinishi, Y., Lund, T. S., Vasilyev, O. V. & Moin, P. 1998 Fully conservative high-order finite difference schemes for incompressible flow. *J. of Comp. Phys.* **143**(1), 90–124.